PIER C

(Received 12 March 2024, Accepted 13 May 2024, Scheduled 25 May 2024)

Reduction of Specific Absorption Rate Using A-Shaped Electromagnetic Band Gap for Quad Port MIMO Antenna

Govindarao Tamminaina and Ramesh Manikonda*

Department of ECE, GITAM University, India

ABSTRACT: This work designs an electromagnetic band gap structure-based quad port rectangular MIMO antenna to operate in the 5G new radio (NR) sub-6 GHz n79 band, with a frequency range of 4.3–5.0 GHz. To achieve optimal radiating element isolation with the least complexity, MIMO antennas' four radiating elements are oriented orthogonally using an A-shaped EBG structure. The electromagnetic band gap (EBG) structure is located between the human phantom model and the MIMO antenna. The MIMO antenna's measurements are $40 \times 40 \times 1.6\,\text{mm}^3$, and it is implemented on an FR-4 substrate with whole ground. Due to EBG structure, the mutual coupling is improved to -26.0 dB. The ECC, DG, and CCL were also calculated. In addition, the specific absorption rate (SAR) value is reduced to 0.22 w/kg. The MIMO antenna is simulated using HFSS software. The vector network analyzer (VNA), model Anritsu MS 2037C is used to measure the various MIMO antenna parameters.

1. INTRODUCTION

Modern wireless communication systems are built around the fundamental technology of multiple-input multiple-output, or MIMO, antennas. They are essential in improving the capacity and performance of wireless networks because they enable the simultaneous transmission and reception of many data streams over a single channel. MIMO technology is widely used in wireless communication standards, including WiFi, 4G LTE, and 5G, to improve data rates, coverage, and network efficiency. Electromagnetic band gap (EBG) structures are renowned for their proficiency in manipulating electromagnetic waves in MIMO antenna design. In this context, they serve dual purposes of reducing antennas' specific absorption rate (SAR) while enhancing their performance. Integrating an EBG structure yields notable SAR reductions [1], with notable values of 0.088 W/kg and 0.070 W/kg at 2.4 GHz and 5.2 GHz, respectively. This MIMO antenna boasts an amazing frequency range of 2 GHz to 30 GHz, an average gain of 3.75 dBi, and a correlation coefficient of 0.5. Article [2] investigates a six-port MIMO antenna that resonantly operates at 4.8 GHz and operates in the mid-bands. Its distinctive geometry combining electromagnetic wave elements, a planar rectangular patch, and several ground enhancements produces remarkable diversity characteristics, such as diversity gains of 9.98 and envelope correlation coefficients less than 0.002. This antenna is suitable for C-band operations, 5G wireless communications applications, wireless local area networks, and n77 bands.

A dual-port, disc-shaped MIMO antenna for ultra-wideband (UWB) systems is discussed in [3]. To improve isolation, an EBG structure is inserted in between the monopole radiators. The antenna exhibits wide impedance bandwidth spanning 120% of the UWB spectrum (3–12 GHz) and achieves a peak gain exceeding 5 dBi across this range. Its compact dimensions and low-profile design make it a notable development. With a fractional bandwidth of roughly 59.76%, a novel compact MIMO antenna arrangement [4] aims to improve wideband gain from 11.5 to 21.3 GHz. This antenna has a $\leq$ 0.00122 envelope correlation coefficient, radiation efficiency between 88.01% and 90.02%, isolation of $\geq$ 24.92 dB, and peak gain of 10.6 dBi. This design feeds two modified Vivaldi radiators with a 1×2 Y-shaped power divider with wideband anti-phase outputs. By acting as a metasurface, a square-ring unit cell reduces backward electromagnetic radiation and directs it forward. Gain is increased over a broad bandwidth due to improved radiation performance in the main lobe direction caused by a U-shaped slot between the radiators.

For the 2.45 and 5.8 GHz ISM frequency bands, a wireless power transfer system with a cubic rectenna MIMO system is designed in [5]. A biocompatible full-package cubic rectenna with circuit modules for data and power regulation is developed using this technology. It uses dual-branch rectifiers for effective energy harvesting and orthogonal circular polarization (CP) to distinguish between two frequency bands. A compact 4×4 MIMO antenna system [6] is integrated into a 5G smartphone with a metal rim. Open and closed stubs, along with bent stubs, are strategically designed within each slit to achieve coverage in the N77 and N79 spectrum bands and minimize mutual coupling between antenna elements. A textile-based microstrip patch antenna tailored for medical applications at 2.4 GHz is introduced in [7]. This antenna minimizes the SAR within the human body EBG layer atop a metasurface, which includes repeating I-shaped structures. A foam layer enhances performance and comfort when being worn on the body.

For 5G communication at 26 GHz, a small and low-profile four-port MIMO antenna [8] is developed. Impedance band-

* Corresponding author: Ramesh Manikonda (rmanikon@gitam.edu).

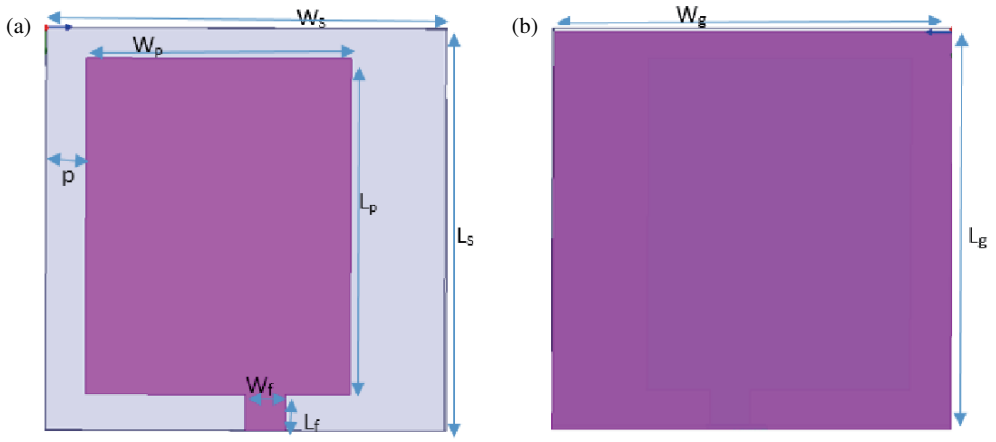

FIGURE 1. Schematic of reference antenna, showing the (a) front and (b) back.

width and isolation are improved by several slot layouts and a defective ground structure (DGS) in the shape of a square. With a large bandwidth and low mutual coupling, this MIMO antenna effectively covers the 5G mm-wave spectrum, improving performance. [9] looks into the application of nanomaterial-based antennas, such as graphene, single-walled carbon nanotubes, and multi-walled carbon nanotubes, in an effort to reduce SAR values. A broad 78% bandwidth (3.2–7.3 GHz) is anticipated to be covered by an eight-element wideband MIMO antenna [10] for 5G mobile terminals with monopole-inspired designs.

An innovative eight-element H-shaped dual-band MIMO antenna [11] is presented for 5G smartphones. The strategic placement of radiating elements minimizes mutual coupling, and the antenna operates efficiently within dual frequency bands, exhibiting impressive bandwidths and pattern diversity. The main PCB's dimensions are $150 \times 75\,\text{mm}^2$, and the side edge frame's measurements are $150 \times 7\,\text{mm}^2$. It functions specifically in the frequency ranges of 3.1–3.78 GHz and 5.43–6.21 GHz, where there is an isolation of more than 12 dB between any two neighboring radiating elements. A different approach, described in [12], focuses on creating a dual-antenna pair for 5G smartphones with a large bandwidth and sound isolation. Utilizing dual-characteristic modes (CMs), this approach achieves broad impedance bandwidth and isolation without external decoupling structures. It extends to an 8×8 MIMO array, providing superior exceeding 20 dB across the 3.3–3.8 GHz operating band. The reduction of SAR in multi-antenna terminals during voice calls is addressed in another innovation [13], by optimizing the relative phase between antenna elements and manipulating power distribution. As long as the device's ground plane has a large enough form factor, this method dramatically lowers SAR while retaining efficiency in a range of frequency bands, from 1.8 to 6 GHz.

Furthermore, SAR reduction in the 8×8 MIMO tablet array is explored in [14, 15], emphasizing the interplay between equalization mode and SAR reduction. This novel approach effectively cancels inverted phase currents, reducing SAR levels and improving isolation performance of 12.94 dB. An EBG structure with a center via is built in the form of a square spiral cell in [16]. This EBG arrangement has enhanced both the overall MIMO system performance and the isolation between antenna elements. The system is well suited for 5G mobile applications thanks to its six antenna elements and wide bandwidth, which spans from 3 GHz to 5 GHz. When the wearable antenna is placed on a denim substrate, the frequency selective surface (FSS) technique in [17] lowers its SAR value to 95.4% compared to not employing FSS. Because the quad-port MIMO antenna in [18] was designed with a metal surface, high isolation and gain were achieved.

2. METHODOLOGY OF QUAD PORT MIMO ANTENNA

2.1. Reference Antenna's Design

Rectangular microstrip antenna design fundamental equations are used to establish the initial design parameters [19]. These settings are then optimized in order to improve performance. Here, h stands for height, and ε_{r} is for the substrate's relative permittivity. L and W, on the other hand, reflect the patch's length and breadth, respectively. Furthermore, the effective permittivity of the substrate is indicated by $\varepsilon_{\text{reff}}$; the resonant frequency is indicated by f_{r}; the length extension on each end is indicated by ΔL; and the velocity of light is indicated by c.

$$W = \frac{c}{2f_r}\sqrt{\frac{2}{\varepsilon_r + 1}} \tag{1}$$

$$\varepsilon_{reff} = \frac{\varepsilon_r + 1}{2} + \frac{\varepsilon_r - 1}{2}\left[1 + 12\frac{h}{W}\right]^{-0.5} \tag{2}$$

$$\frac{\Delta L}{h} = 0.412\frac{(\varepsilon_{reff} + 0.3)(\frac{W}{h} + 0.264)}{(\varepsilon_{reff} - 0.258)(\frac{W}{h} + 0.8)} \tag{3}$$

$$L = \frac{c}{2f\sqrt{\varepsilon_{reff}}} - 2\Delta L \tag{4}$$

The single patch antenna is designed using $\varepsilon_r = 4.4$, FR-4 substrate with a thickness of 1.6 mm on the whole ground. Fig. 1(a) and Fig. 1(b) show the front and back views of the reference antenna. The design parameters of a single patch antenna are shown in Table 1. The reflection coefficient of a

TABLE 1. The specifications for the proposed structure.

Parameter	L_g	W_g	L_s	W_s	L_p	W_p	L_f	W_f	P
Value (mm)	20	20	20	20	16.7	13.2	2	1.8	1.5

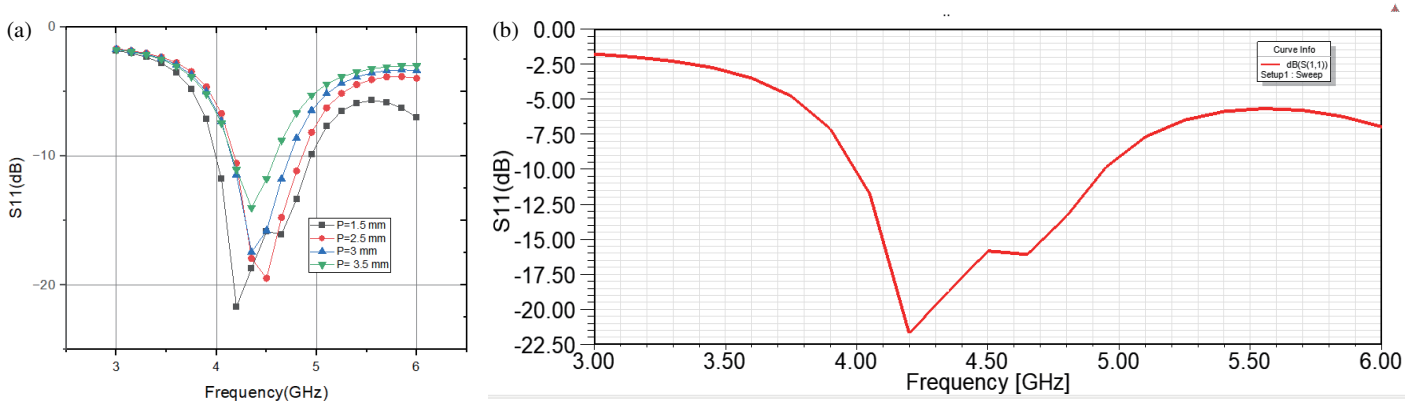

FIGURE 2. S_{11} of reference antenna using (a) parametric analysis (b) at $p = 1.5$ mm.

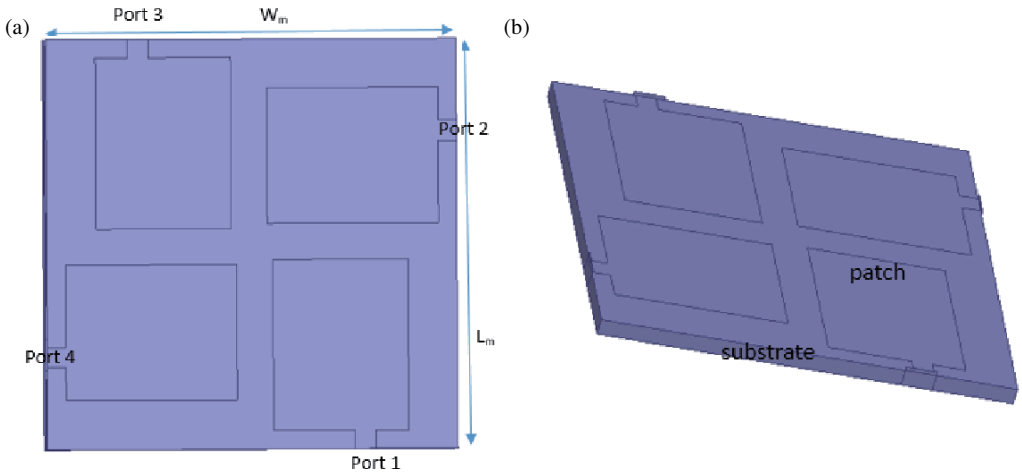

FIGURE 3. Quad port MIMO antenna without EBG (a) front view and (b) side view.

single patch antenna is displayed in Fig. 2 utilizing parametric analyses 2(a) and 2(b), which show the reflection coefficient (S_{11}) at $p = 1.5$ mm for the desired frequency band. The p is a gap between the patch and the edge of the substrate changed from 1.5 to 3.5 mm, and 1.5 mm is the space between them; it is given a better reflection coefficient of -21.0 dB.

2.2. Design of Quad Port MIMO Antenna

A reference antenna is incorporated into the design of the four-port MIMO antenna. As shown in Fig. 3(a), these four antennas are positioned orthogonally, and its dimensions are $L_m = 40$ mm and $W_m = 40$ mm. Fig. 3(b) shows the side view of the four-port MIMO antenna without an electromagnetic band gap (EBG), and it consists of a three layer patch, a substrate, and ground. The single EBG structure is seen from the front view in Fig. 4(a), which is positioned on a 1.6 mm-thick FR-4 substrate. The length of EBG is $L_e = 12$ mm, and width of EBG is $W_e = 10.5$ mm, $b = 2.5$ mm, $e = 1$ mm. They are dimensions of the EBG. The 3×3 EBG array is seen from the front view in Fig. 4(b). The gap between adjacent EBG cells is a vertical gap $x = 0.8$ mm and horizontal gap $y = 2.7$ mm, respectively.

Figure 5(a) shows the reflection phase of the EBG cell using parametric analysis, and it is used to choose the value of e. The width e is changed from 0.4 mm to 1.8 mm and selected for the desired frequency range; the value is $e = 1$ mm. Fig. 5(b) depicts the reflection phase of an A-shaped EBG cell at $e = 1$ mm. The A-shaped EBG acts as a band gap that creates a stopband to block electromagnetic waves of specific frequency bands. The EBG structure suppresses the surface waves and reduce mutual coupling effect. The integration of an A-shaped EBG array with a four-port MIMO antenna is demonstrated in Fig. 6(a). The layer side perspective of the MIMO antenna is displayed in Fig. 6(b). The 1 mm thick foam is positioned between the EBG array and MIMO antenna. The A-shaped EBG structure is placed on an FR-4 substrate (1.6 mm). The slot length of the EBG cell is $L_{sl} = 6$ mm, and width is 2.5 mm.

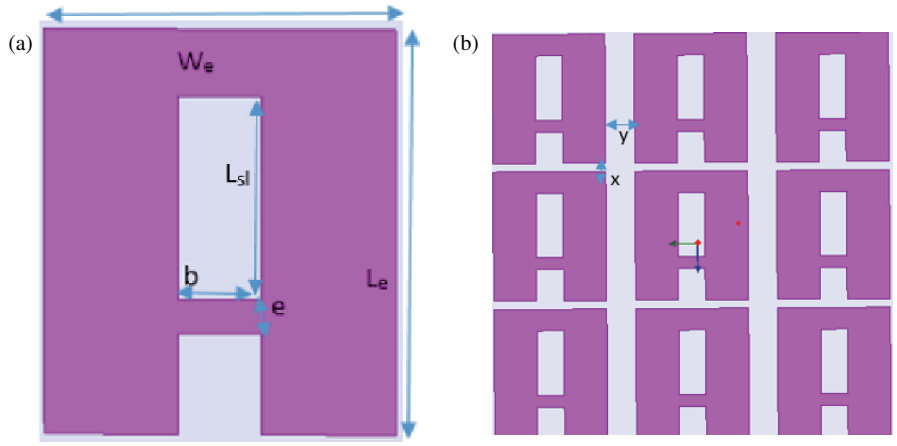

FIGURE 4. (a) single EBG structure front view and (b) 3×3 EBG array front view.

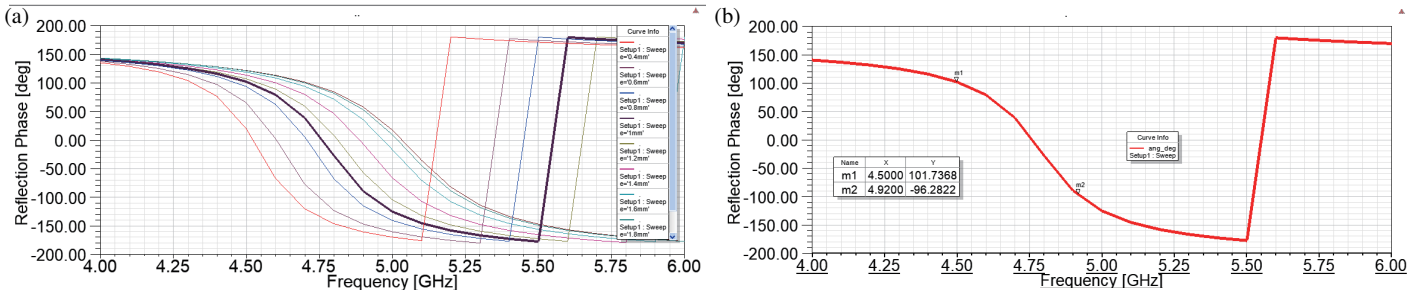

FIGURE 5. Reflection phase of EBG (a) using parametric analysis, and (b) at $e = 1$ mm.

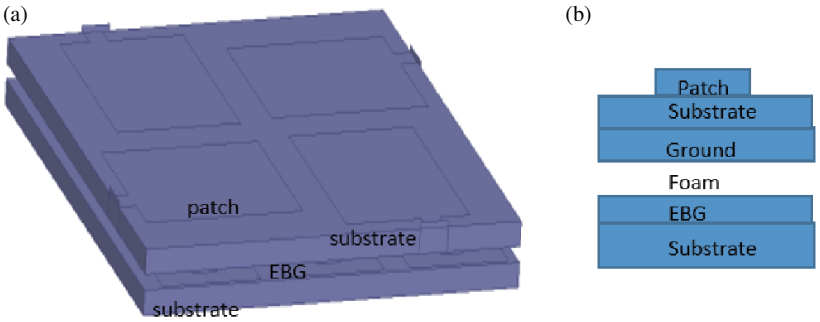

FIGURE 6. Quad port MIMO antenna with EBG, (a) front and (b) layer side view.

3. RESULTS AND DISCUSSIONS

The reflection coefficient of the four-port MIMO antenna is shown in Fig. 7(a) both with and without an EBG construction. In particular, between 4.4 and 5 GHz, the MIMO antenna with an A-shaped EBG maintains a reflection coefficient below -10 dB. Furthermore, throughout the intended frequency range, the MIMO antenna's transmission coefficient is less than -25.0 dB without EBG and -26.0 dB with EBG at ports between 1 and 3 (S_{13}). Because the A-shaped EBG structure is positioned below the ground structure below the MIMO antenna, its presence has less effect on the transmission and reflection coefficients here.

Since envelope correlation coefficient (ECC) is one of the primary performance metrics of a MIMO antenna system, many parameters are employed to analyze the performance of the MIMO antenna [20–22]. It can be calculated using the equation below, and it is the S-parameters method. The return loss and isolation parameters are used in the calculation of ECC value.

$$\mathrm{ECC} = \frac{\left|S_{ii} * S_{ij} + S_{ji} * S_{jj}\right|^2}{\left(1 - \left|S_{ii}\right|^2 - \left|S_{ji}\right|^2\right) * \left(1 - \left|S_{jj}\right|^2 - \left|S_{ij}\right|^2\right)} \tag{5}$$

In order to preserve the wireless system's quality and dependability, the MIMO antenna's diversity gain (DG) needs to be strong. Additionally, it is computed by

$$\mathrm{DG} = 10\sqrt{1 - (\mathrm{ECC})^2} \tag{6}$$

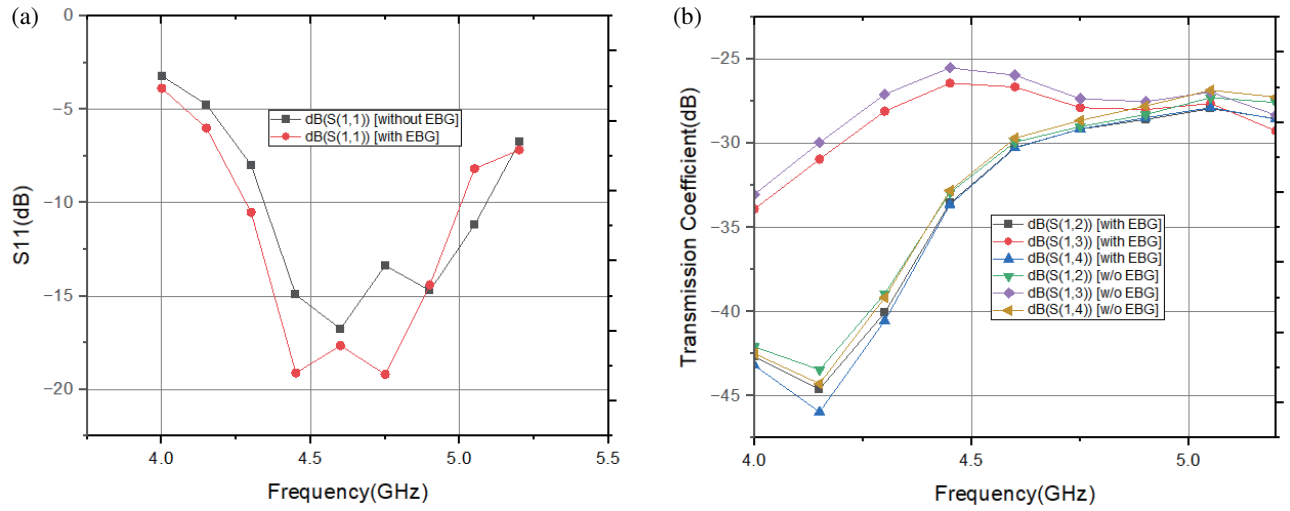

FIGURE 7. Four port MIMO antenna with and without EBG of (a) Reflection, (b) Transmission Coefficient.

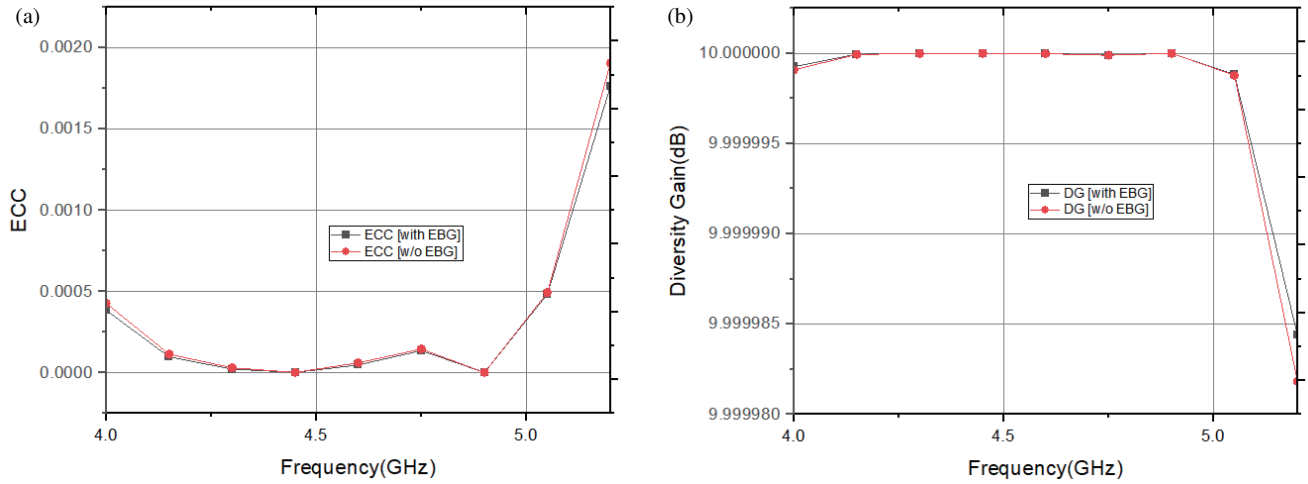

FIGURE 8. (a) ECC (b) DG of four port MIMO antenna.

One further crucial characteristic for the MIMO system is channel capacity loss (CCL), which should have a value of less than 0.4 bits/s/Hz. Use this formula to determine capacity loss,

$$\mathrm{CCL} = -\log_2(\varphi^R) \tag{7}$$

Here, φ^R is the correlation matrix of the receiving antenna, which is expressed as follows.

$$(\varphi^R) = \begin{matrix} \varphi_{ii} & \varphi_{ij} \\ \varphi_{ji} & \varphi_{jj} \end{matrix} \tag{8}$$

Here , $\varphi_{ii} = 1 - (|S_{ii}|^2 + |S_{ij}|^2)$, $\varphi_{jj} = 1 - (|S_{jj}|^2 + |S_{ji}|^2)$, $\varphi_{ij} = -(S_{ii} * S_{ij} + S_{ji} * S_{jj})$ and $\varphi_{ji} = -(S_{jj} * S_{ji} + S_{ij} * S_{ii})$.

For the suggested frequency range depicted in Fig. 8(a), the ECC value of the four-port MIMO antenna, both with and without an EBG structure, is less than 0.0004. Fig. 8(b) displays the DG value exceeding 9.99, both with and without EBG structure.

As seen in Fig. 9(a), the CCL value is less than 0.2 bits/s/Hz both with and without the EBG structure of the MIMO antenna. The efficiency of the four-port MIMO antenna, both with and without EBG, is in Fig. 9(b). The efficiency for the suggested frequency band is between 0.75 and 0.79. The Fig. 10(a) shows the MIMO antenna without EBG, and Fig. 10(b) shows that with A-shaped EBG on human phantom model. The phantom model is built using layers that are correspond to muscle, fat, and skin and is optimized for a 4.6 GHz frequency. The precise values corresponding to these tissue layers are given in Table 2 [23].

SAR highlights the quantity of electromagnetic energy that the human body's tissue can absorb when it is exposed to the radiation source [24], where σ is the conductivity, E the electric field intensity, and ρ the mass density of the tissue. The SAR value is calculated by the following equation

$$\mathrm{SAR} = \frac{\sigma E^2}{\rho} \tag{9}$$

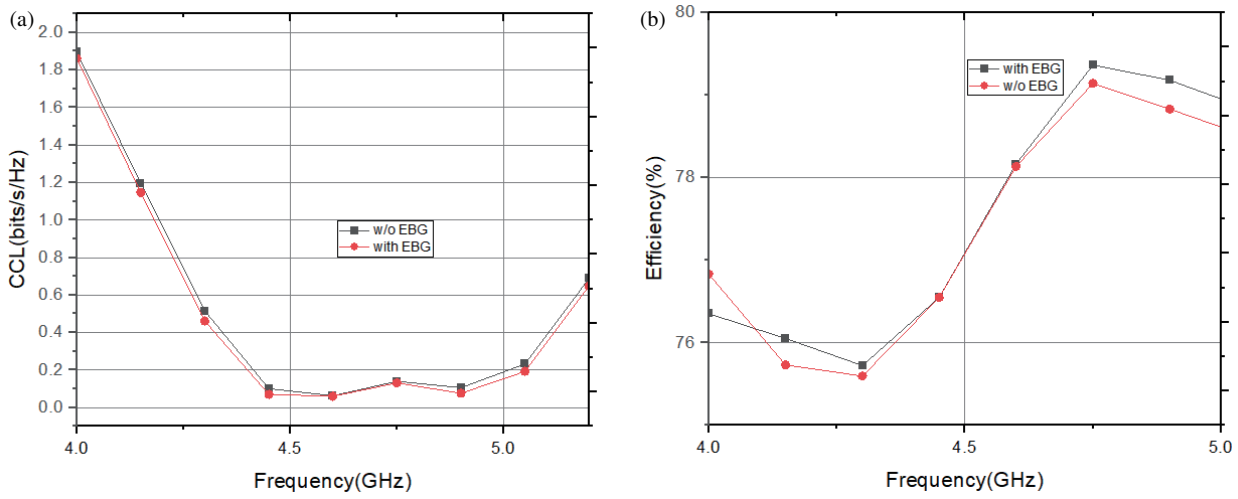

FIGURE 9. Four port MIMO antenna (a) CCL (b) Efficiency, with and without EBG.

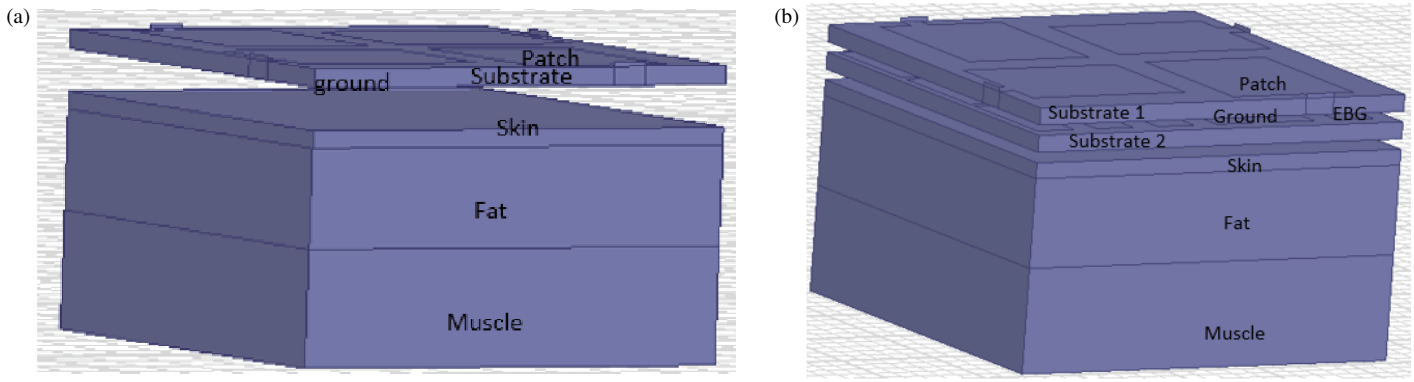

FIGURE 10. Quad port MIMO antenna on human phantom model (a) without (b) with EBG.

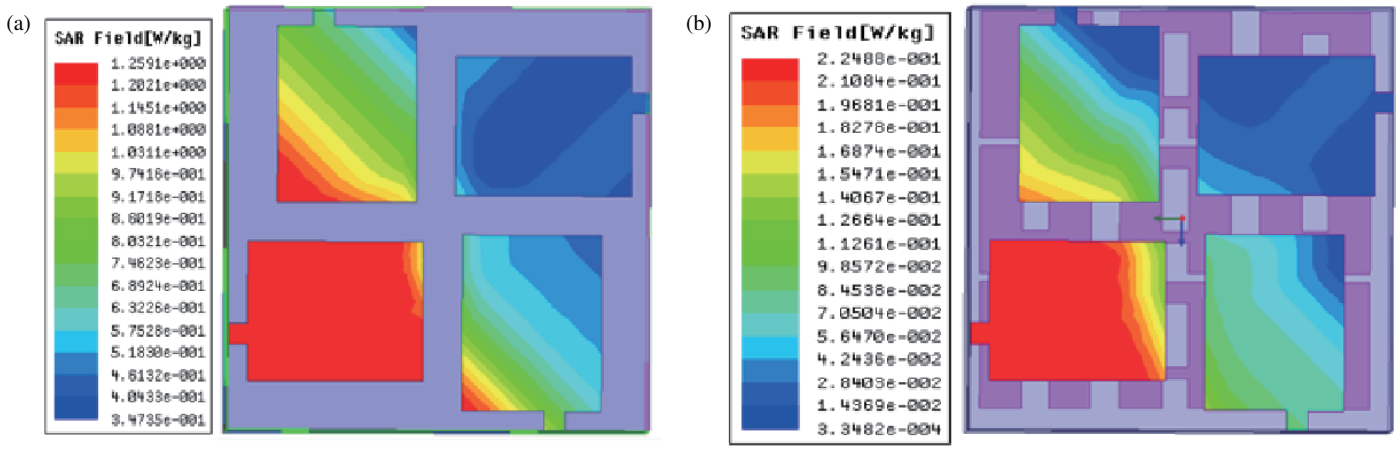

FIGURE 11. SAR of MIMO antenna (a) without (b) with EBG.

The SAR value should, on average, be less than 2.0 W/kg over 10 g of tissue, in accordance with European regulations. Without the EBG, Fig. 11(a) shows an average SAR value of 1.25 W/kg; Fig. 11(b) shows a SAR value of 0.22 W/kg over the 10 g of tissue with the EBG included into the suggested MIMO antenna on the human phantom model. As a result of the A-shaped EBG construction, SAR has decreased from 1.25 to 0.22 W/kg. Interestingly, the EBG structure is placed in between the phantom model and the MIMO antenna. The performance characteristics of the recommended MIMO antenna are contrasted with those of other antennas in Table 3.

TABLE 2. The specifications of the human phantom model at 4.6 GHz.

Tissues	Thickness (mm)	Conductivity [S/m]	Relative permittivity	Loss tangent
Skin	1	2.68	36.18	0.29
Fat	5	0.21	5.07	0.16
Muscle	6	3.51	50.18	0.27

TABLE 3. Comparing the suggested MIMO antenna to alternative antennas.

Ref	No. Ports	Size (mm^2)	Frequency range (GHz)	Isolation (dB)	ECC	Efficiency (%)
[25]	5	80×80	4.5–5.0	> -15	< 0.01	NA
[26]	4	112×112	5.1–5.3	> -22	< 0.15	89
[27]	4	30×30	4.8–6.0	> -10	< 0.15	67
[28]	4	56×56	4.5–5.1	> -20	< 0.01	87
[29]	4	40×40	4.7–5.1	> -25	< 0.01	70
[Pro. Ant]	4	40×40	4.4–5.0	> -26	< 0.0005	78

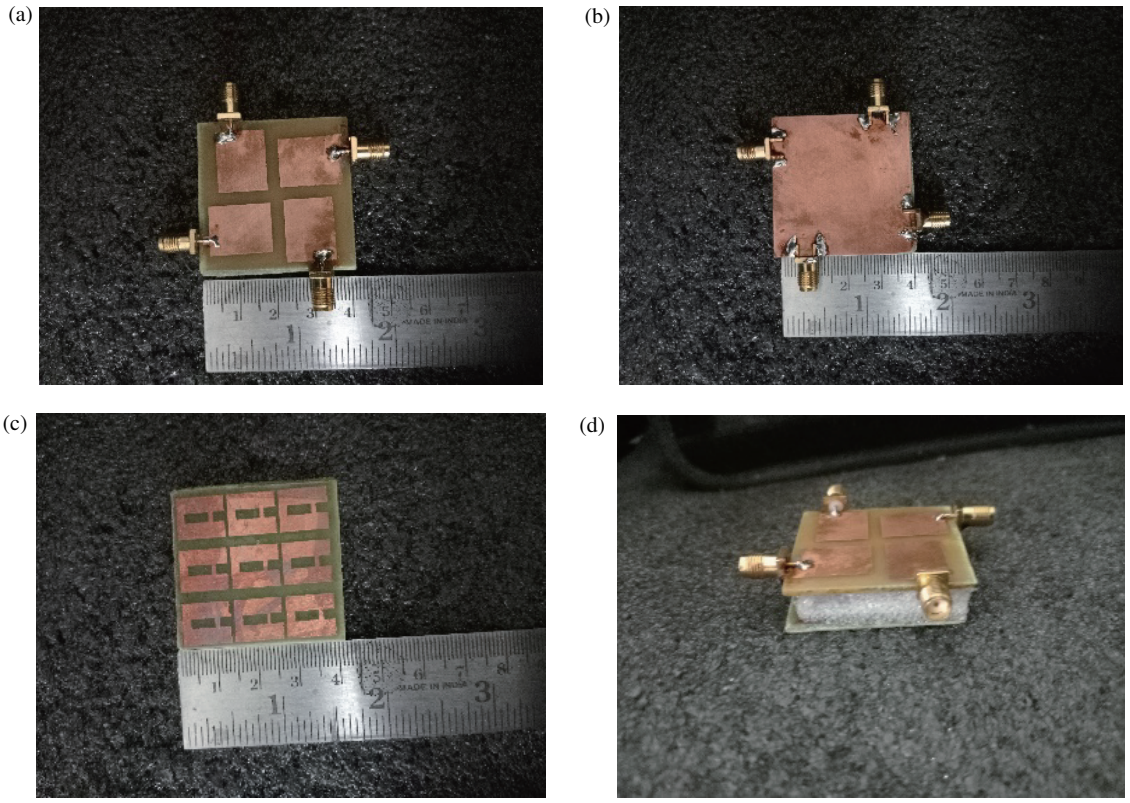

FIGURE 12. Fabrication of quad port MIMO antenna (a) front (b) back (c) EBG (d) Top view.

The quad-port MIMO antenna prototype with an electromagnetic band gap (EBG) structure is shown in Fig. 12. In particular, the front and back views of the MIMO antenna and the front view of the EBG array are shown in Figs. 12(a), 12(b), and 12(c), respectively. As shown in Fig. 12(d), the overall assembly, 1 mm thick layer of foam is kept between the MIMO antenna and the EBG array. Figs. 13(a) and 13(b) present the measured and simulated results of the proposed quad-port MIMO

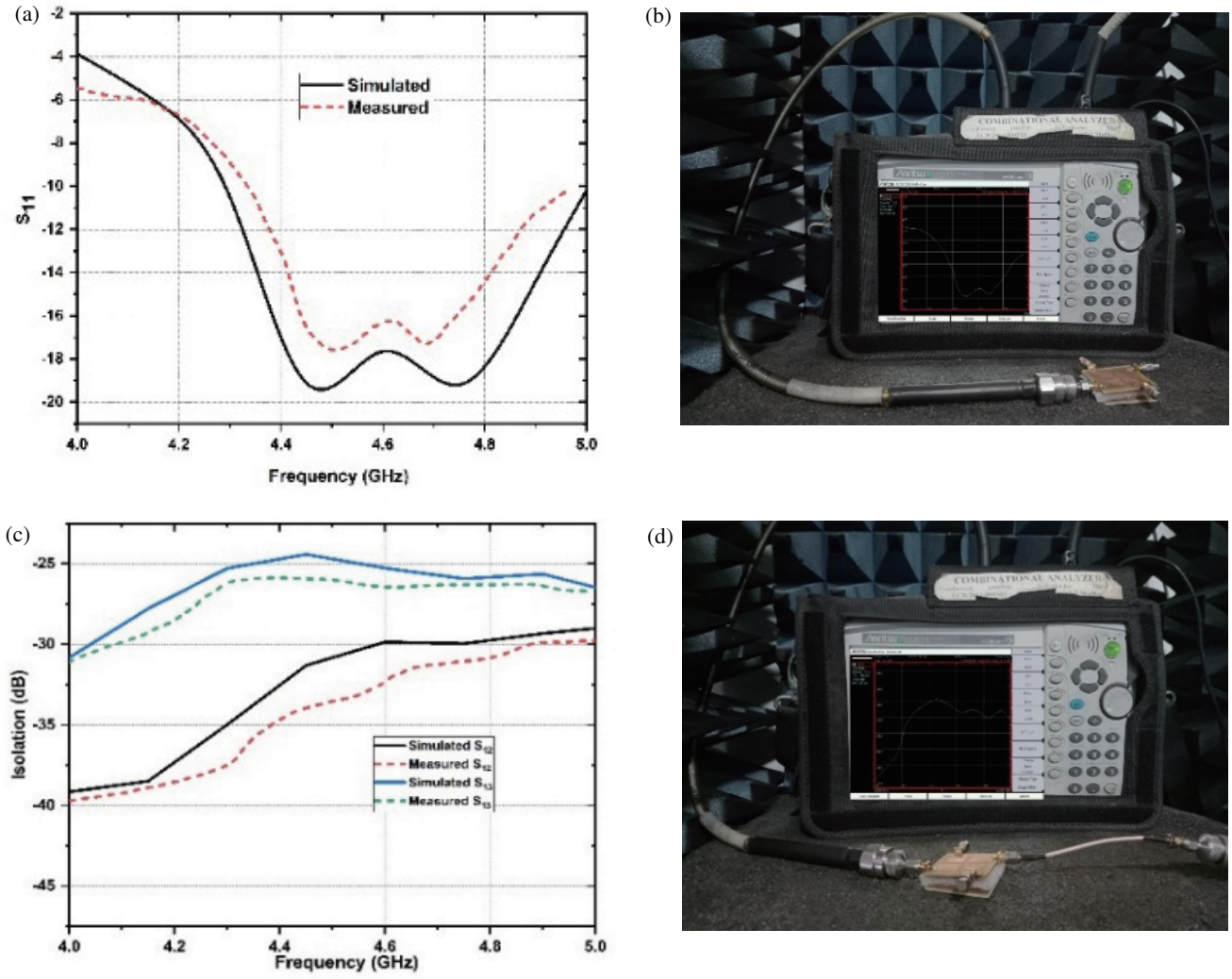

FIGURE 13. MIMO antenna with EBG simulated and measured (a), (b) S_{11}, and (c), (d) Isolation.

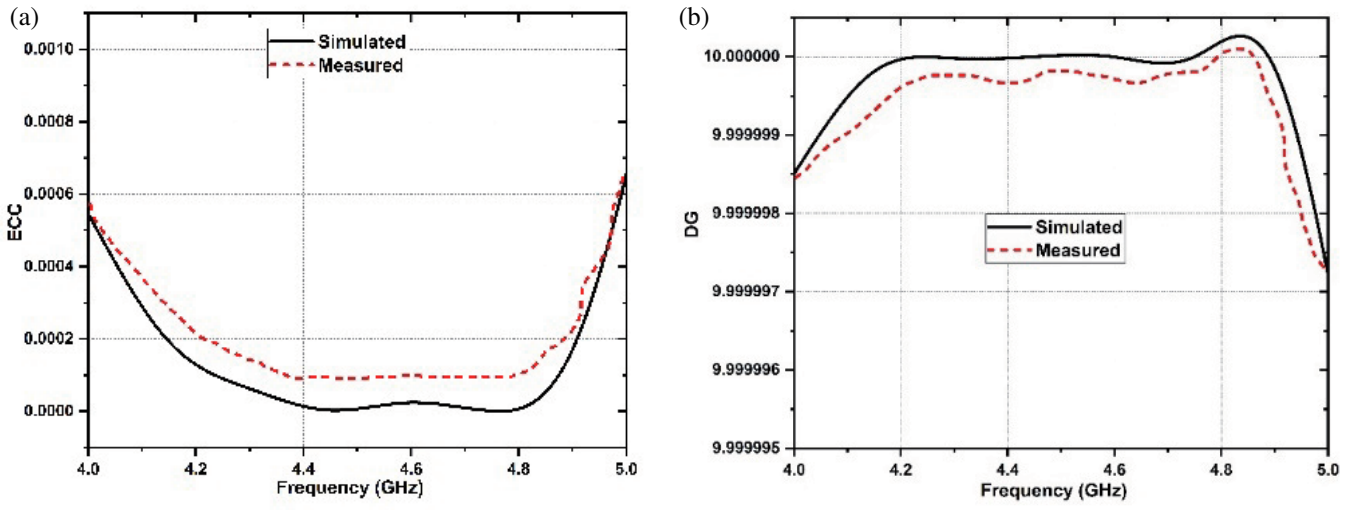

FIGURE 14. MIMO antenna with EBG measured. (a) ECC, (b) DG.

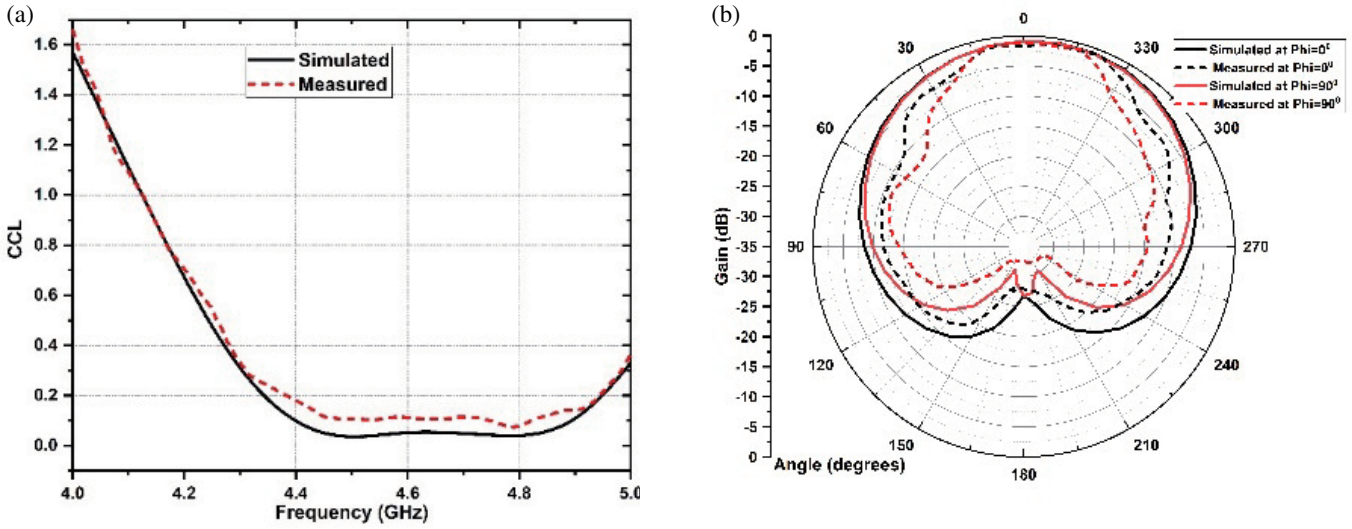

FIGURE 15. MIMO antenna with EBG measured. (a) CCL, (b) Radiation Pattern.

antenna with the EBG structure for S_{11}. Figs. 13(c) and 13(d) show the isolation between ports 1 and 3, $S_{13} => -26.0$, and various isolations. Fig. 14(b) shows the observed directivity gain (DG) value of 9.99 dB, whereas Fig. 14(a) shows that the measured ECC value is less than 0.0002. Furthermore, for the suggested frequency range of 4.4–5.0 GHz, Fig. 15(a) shows a measured CCL of less than 0.2, and Fig. 15(b) shows the associated radiation pattern. Notably, the measured results validate the calculated findings, proving the effectiveness of the suggested MIMO antenna.

4. CONCLUSION

The quad-port MIMO antenna is appropriate for n79 band 5G communication since it runs in the 4.4–5.0 GHz frequency range and is improved with an A-shaped electromagnetic band gap (EBG) structure on a human phantom model. The performance of the MIMO antenna with EBG is significantly improved compared to that without the EBG structure. Effective mutual coupling is shown by the -26.0 dB between ports 1 and 3. Additionally, the antenna's remarkable 78% efficiency and ECC value of less than 0.0002 demonstrate its improved isolation, efficiency, and appropriateness for 5G communication applications. With the EBG structure, the CCL is less than 0.05 bits/s/Hz, indicating little interference across signal lines. Furthermore, for the suggested MIMO antenna with the EBG positioned on the human phantom model, the specific absorption rate (SAR) value is significantly decreased to 0.22 W/kg across 10 g of tissue. These observed results successfully verify the MIMO antenna's simulated performance parameters, confirming its efficacy and appropriateness for 5G communication applications. In future, the four port MIMO antenna using a multiband EBG structure can be expanded to the multiband 5G applications like N77/N78/N79 bands.

REFERENCES

[1] Kumkhet, B., P. Rakluea, N. Wongsin, P. Sangmahamad, W. Thaiwirot, C. Mahatthanajatuphat, and N. Chudpooti, "SAR reduction using dual band EBG method based on MIMO wearable antenna for WBAN applications," *AEU — International Journal of Electronics and Communications*, Vol. 160, 154525, 2023.

[2] Kumar, A., J. Mohanty, P. Pattanayak, D. Sabat, and G. Prasad, "Six-port mid-bands low-SAR MIMO antenna for WLAN, 5G mobile terminals, and C-band applications," *AEU — International Journal of Electronics and Communications*, Vol. 166, 154665, 2023.

[3] Babu, N. S., A. Q. Ansari, B. K. Kanaujia, G. Singh, and S. Kumar, "A two-port UWB MIMO antenna with an EBG structure for WLAN/ISM applications," *Materials Today: Proceedings*, Vol. 74, 334–339, 2023.

[4] Wang, W., Z. Fang, K. Tang, X. Wang, Z. Shu, Z. Zhao, and Y. Zheng, "Wideband gain enhancement of MIMO antenna and its application in FMCW radar sensor integrated with CMOS-based transceiver chip for human respiratory monitoring," *IEEE Transactions on Antennas and Propagation*, Vol. 71, No. 1, 318–329, Jan. 2023.

[5] Kaim, V., N. Singh, B. K. Kanaujia, L. Matekovits, K. P. Esselle, and K. Rambabu, "Multi-channel implantable cubic rectenna MIMO system with CP diversity in orthogonal space for enhanced wireless power transfer in biotelemetry," *IEEE Transactions on Antennas and Propagation*, Vol. 71, No. 1, 200–214, Jan. 2023.

[6] Ahn, J., Y. Youn, B. Kim, J. Lee, N. Choi, Y. Lee, G. Kim, and W. Hong, "Wideband 5G N77/N79 4 × 4 MIMO antenna featuring open and closed stubs for metal-rimmed smartphones with four slits," *IEEE Antennas and Wireless Propagation Letters*, Vol. 22, No. 12, 2798–2802, Dec. 2023.

[7] Kavitha, K., S. R. V. Gokul, S. Yazhini, J. M. K. Durga, and R. Keerthana, "EBG Integrated Metasurface Antenna for SAR Reduction," *Progress In Electromagnetics Research C*, Vol. 135, 227–240, 2023.

[8] Güler, C. and S. E. B. Keskin, "A novel high isolation 4-Port compact MIMO antenna with DGS for 5G applications," *Micromachines*, Vol. 14, No. 7, 1309, 2023.

[9] Stephen, J. P. and D. J. Hemanth, "SAR reduction in human head phantom using nanomaterial MIMO antenna," *Progress In Electromagnetics Research Letters*, Vol. 108, 103–112, 2023.

[10] Rai, A. K., R. K. Jaiswal, K. Kumari, K. V. Srivastava, and C.-Y.-D. Sim, "Wideband monopole eight-element MIMO antenna for 5G mobile terminal," *IEEE Access*, Vol. 11, 689–696, 2022.

[11] Zahid, M. N., Z. Gaofeng, S. H. Kiani, U. Rafique, S. M. Abbas, M. Alibakhshikenari, and M. Dalarsson, "H-shaped eight-element dual-band MIMO antenna for sub-6 GHz 5G smartphone applications," *IEEE Access*, Vol. 10, 85 619–85 629, 2022.

[12] Hu, W., Z. Chen, L. Qian, L. Wen, Q. Luo, R. Xu, W. Jiang, and S. Gao, "Wideband back-cover antenna design using dual characteristic modes with high isolation for 5G MIMO smartphone," *IEEE Transactions on Antennas and Propagation*, Vol. 70, No. 7, 5254–5265, Jul. 2022.

[13] Jamshed, M. A., T. W. C. Brown, and F. Héliot, "Dual antenna coupling manipulation for low SAR smartphone terminals in talk position," *IEEE Transactions on Antennas and Propagation*, Vol. 70, No. 6, 4299–4306, Jun. 2022.

[14] Fang, Y., Y. Liu, Y. Jia, Y. Xu, and B. Lai, "5G SAR-reduction MIMO antenna with high isolation for full metal-rimmed tablet device," *IEEE Transactions on Antennas and Propagation*, Vol. 70, No. 5, 3846–3851, May 2022.

[15] Zhang, H. H., G. G. Yu, X. Z. Liu, G. S. Cheng, Y. X. Xu, Y. Liu, and G. M. Shi, "Low-SAR MIMO antenna array design using characteristic modes for 5G mobile phones," *IEEE Transactions on Antennas and Propagation*, Vol. 70, No. 4, 3052–3057, Apr. 2022.

[16] Hediya, A. M., A. M. Attiya, and W. S. El-Deeb, "5G MIMO antenna system based on patched folded antenna with EBG substrate," *Progress In Electromagnetics Research M*, Vol. 109, 149–161, 2022.

[17] SAGNE, D. and R. A. PANDHARE, "SAR reduction of wearable SWB antenna using FSS for wireless body area network applications," *Sādhanā*, Vol. 49, No. 1, 76, 2024.

[18] Hasan, M. M., M. T. Islam, M. Samsuzzaman, M. H. Baharuddin, M. S. Soliman, A. Alzamil, I. I. M. A. Sulayman, and M. S. Islam, "Gain and isolation enhancement of a wideband MIMO antenna using metasurface for 5G sub-6 GHz communication systems," *Scientific Reports*, Vol. 12, No. 1, 9433, 2022.

[19] Tamminaina, G. and R. Manikonda, "Investigation on performance of four port MIMO antenna using electromagnetic band gap for 5G communication," *Progress In Electromagnetics Research M*, Vol. 119, 51–62, 2023.

[20] Gabriel, C., "Compilation of the dielectric properties of body tissues at RF and microwave frequencies," King's College London, Department of Physics, United Kingdom, Tech. Rep., 1996.

[21] Megahed, A. A., M. Abdelazim, E. H. Abdelhay, and H. Y. M. Soliman, "Sub-6 GHz highly isolated wideband MIMO antenna arrays," *IEEE Access*, Vol. 10, 19 875–19 889, 2022.

[22] Yadav, D., M. P. Abegaonkar, S. K. Koul, V. N. Tiwari, and D. Bhatnagar, "Two element band-notched UWB MIMO antenna with high and uniform isolation," *Progress In Electromagnetics Research M*, Vol. 63, 119–129, 2018.

[23] Hasan, M. N., S. Chu, and S. Bashir, "A DGS monopole antenna loaded with U-shape stub for UWB MIMO applications," *Microwave and Optical Technology Letters*, Vol. 61, No. 9, 2141–2149, 2019.

[24] Stephen, J. P. and D. J. Hemanth, "SAR reduction in human head phantom using nanomaterial MIMO antenna," *Progress In Electromagnetics Research Letters*, Vol. 108, 103–112, 2023.

[25] Jaiswal, R. K., K. Kumari, A. K. Ojha, and K. V. Srivastava, "Five-port MIMO antenna for n79-5G band with improved isolation by diversity and decoupling techniques," *Journal of Electromagnetic Waves and Applications*, Vol. 36, No. 4, 542–556, 2022.

[26] Yang, M. and J. Zhou, "A compact pattern diversity MIMO antenna with enhanced bandwidth and high-isolation characteristics for WLAN/5G/WiFi applications," *Microwave and Optical Technology Letters*, Vol. 62, No. 6, 2353–2364, Jun. 2020.

[27] Das, G., N. K. Sahu, A. Sharma, R. K. Gangwar, and M. S. Sharawi, "FSS-based spatially decoupled back-to-back four-port MIMO DRA with multidirectional pattern diversity," *IEEE Antennas and Wireless Propagation Letters*, Vol. 18, No. 8, 1552–1556, Aug. 2019.

[28] Sharma, S. and M. Kumar, "Design and analysis of a 4-port MIMO microstrip patch antenna for 5G mid band applications," *Progress In Electromagnetic Research C*, Vol. 129, 231–243, 2023.

[29] Ali, H., X.-C. Ren, I. Bari, M. A. Bashir, A. M. Hashmi, M. A. Khan, S. I. Majid, N. Jan, W. U. K. Tareen, and M. R. Anjum, "Four-port MIMO antenna system for 5G n79 band RF devices," *Electronics*, Vol. 11, No. 1, 35, 2022.